Measles Epidemics in Vaccinated Populations

Katherine Broadfoot[1] and Matt Keeling[2]

[1]Centre for Complexity Science, University of Warwick
[2]WIDER Centre, Mathematics Institute and School of Life Sciences, University of Warwick

Abstract

The high infectivity of Measles and the serious complications it can lead to motivate the pressing need to understand the cause of outbreaks. Here, we use bifurcation diagrams as a tool to compare age structured, seasonally forced models and find that when sinusoidal seasonal forcing is used, the fractional ageing model exhibits chaotic dynamics for large enough amplitudes of seasonality whereas the cohort ageing model only produces annual or biennial dynamics for all amplitudes. When a term-time seasonal forcing equation is used, the fractional ageing model does not exhibit chaotic dynamics for the parameters considered, whereas with the cohort ageing model, period doubling leads to chaotic dynamics for sufficiently large amplitudes of seasonality. The cohort ageing model was then fitted to data from the 2013 outbreak in Swansea, which produces very regular annual dynamics for all amplitudes of seasonality.

1 Introduction

Measles is a highly contagious disease – before the introduction of vaccination more than 90% of individuals were infected before they were 10 years old [38] – which has serious associated complications such as pneumonia, encephalitis, hepatitis, acute diarrhoea and death [25, 30]. Measles is no longer endemic in countries such as the USA, Finland and the UK due to successful vaccination campaigns [8, 26, 28]. However, the disease does remain endemic elsewhere, and so regions which are Measles free remain at risk of outbreaks from imports of the disease [34]. Despite the vaccine being highly effective [6], elimination of Measles is particularly difficult due to its high basic reproductive ratio, R_0. The basic reproductive ratio is the average number of secondary infections from the primary infection of a single individual in a susceptible population [3], and is estimated to be approximately 14–18 for Measles in England and Wales [1]. Taking $R_0 = 17$, this gives a critical minimum vaccination level [10] of $V_c = 1 - 1/R_0 \approx 94\%$ for a homogeneous population. The World Health Organisation (WHO) therefore recommends a vaccination level of at least 93–95% for regions aiming to eliminate Measles [38].

The vaccination level for one year olds was 93% in the UK and 91% in the US according to WHO data from 2014 [37]. In the UK this is a significant rise from the levels is the late 90s/ early 2000s (just 81% in 2004) which is generally attributed to the scare surrounding links between the measles, mumps and rubella (MMR) vaccine and autism [5, 23]. The recent large outbreak in Swansea in 2013 [15] has been linked to the low vaccine uptake during the height of the MMR scare [16, 23, 29, 36]. There have also been recent large outbreaks in California [22] and Ohio [14], but none in London which has a much lower vaccination uptake level than the rest of the UK ($\approx 88\%$ compared to $\approx 95\%$ for the whole of England [27]).

Measles has been modelled extensively, with a range of models based on the SEIR compartmental model [20] which has been refined to include features such as age structure [2, 31], seasonal forcing [4, 9, 19] and spatial structure [17, 24]. However, further work is necessary to understand the cause of outbreaks in relatively high vaccination areas such as Swansea when London continues to go without an outbreak. Here, we compare age structured, seasonally forced models using bifurcation diagrams and then incorporate data from the 2013 Swansea outbreak in an attempt to better understand its causes.

2 Age structured models for Measles

The traditional SEIR model [20] is a compartmental model in which the population is split into four compartments: S, E, I and R. These represent the number of individuals who are susceptible, exposed but not yet infectious, infectious and recovered, respectively, and the movement between these classes is governed by a set of ordinary differential equations. We consider a more realistic model for Measles by including age structure in the SEIR model. Each compartment is split into n age classes, so that S_a, E_a, I_a and R_a are the number of susceptible, exposed, infectious and recovered individuals, respectively, in age class a. The dynamics of the system are then governed by the equations

$$\begin{aligned}
\frac{dS_a}{dt} &= B_a N_n - \sum_b \beta_{ab} I_b S_a / N - d_a S_a, \\
\frac{dE_a}{dt} &= \sum_b \beta_{ab} I_b S_a / N - \sigma E_a - d_a E_a, \\
\frac{dI_a}{dt} &= \sigma E_a - \gamma I_a - d_a I_a, \\
\frac{dR_a}{dt} &= \gamma I_a - d_a R_a,
\end{aligned} \tag{1}$$

where β is the who acquires infection from whom (WAIFW) matrix governing interactions between susceptible and infectious individuals, such that the element β_{ab} is the level of interaction between susceptible individuals in age class a and infected individuals in age class b. The average latency period is $1/\sigma$, the average infectious period is $1/\gamma$, B_a is the birth rate into age class a and d_a is the death rate of individuals in age class a. The total population size $S + E + I + R = N$ is kept constant by setting the birth rate to be

$$B_a = \begin{cases} B, & \text{if } a = 1, \\ 0, & \text{otherwise,} \end{cases} \tag{2}$$

and the death rate to

$$d_a = \begin{cases} B, & \text{if } a = n, \\ 0, & \text{otherwise.} \end{cases} \tag{3}$$

Therefore births only occur into the first age class of susceptibles, and deaths occur from the final age class of all states. Throughout, the values $\sigma = 1/8$, $\gamma = 1/5$ (corresponding to an exposed period of 8 days and infectious period of 5 days) and $B = 1/(55 \times 365)$ are used.

2.1 Fractional ageing model

In this model the population is split into four coarse age classes corresponding to pre-school (0–4 years old), primary school (5–11 years old), secondary school (12–18 years old) and adults (18+ years old). The WAIFW matrix, β, then takes the form below to give realistic mixing between the age groups, with $\beta_1 = 2.089$, $\beta_2 = 9.336$, $\beta_3 = 2.086$ and $\beta_4 = 2.037$ [18].

$$\beta = \begin{pmatrix} \beta_1 & \beta_1 & \beta_3 & \beta_4 \\ \beta_1 & \beta_2 & \beta_3 & \beta_4 \\ \beta_3 & \beta_3 & \beta_3 & \beta_4 \\ \beta_4 & \beta_4 & \beta_4 & \beta_4 \end{pmatrix} \tag{4}$$

Ageing once a year moves a fraction of each group into the next, so that the number of susceptibles updates as:

$$\begin{aligned} S_1 &\to S_1 - S_1/5, \\ S_2 &\to S_2 + S_1/5 - S_2/6, \\ S_3 &\to S_3 + S_2/6 - S_3/6, \\ S_4 &\to S_4 + S_3/6 \end{aligned}$$

and the number of exposed, infectious and recovered individuals update in the same way.

Analyses of case report time series has shown that the transmission of Measles is seasonally dependent, with much lower levels during school holidays [11, 12, 21, 32, 39]. Seasonal forcing is usually incorporated into an SEIR model through the transmission rate, either using a sinusoidal term [4] or a square wave term, which is high during term time and low during holidays [7, 9, 19]. To add seasonal forcing to the age structured models, β_2, the term governing interaction between school age children becomes time dependent. For the sinusoidal forcing term, we take this to be

$$\beta_2(t) = \hat{\beta}\left(1 + b\sin(2\pi t/365)\right), \tag{5}$$

where $b \in [0, 1]$ so $\beta_2(t) \geq 0$ for all t and for the square wave term,

$$\beta_2(t) = \hat{\beta}\left(1 + b\right)^{\mathrm{Term}(t)}, \tag{6}$$

where $b \geq -1$, although throughout we will consider $b \in [0, 1]$ for ease of comparison with the sinusoidal forcing term, and

$$\mathrm{Term}(t) = \begin{cases} -1, & \text{during school holidays,} \\ 1, & \text{otherwise.} \end{cases} \tag{7}$$

The value $\hat{\beta}$ is the constant value of β_2 before seasonal forcing is introduced, and b is the amplitude of seasonality. To allow comparison of the seasonal forcing methods, bifurcation diagrams were produced by varying the amplitude of seasonality, b. Given the same initial conditions at $b = 0$, the equations were numerically integrated for 10,000 years to allow the assumption that an asymptotic state has been reached and the total number of infectious individuals plotted against the current amplitude of seasonality at the beginning of the calendar year (January), and at the beginning of the epidemiological year (September) for 50 years.

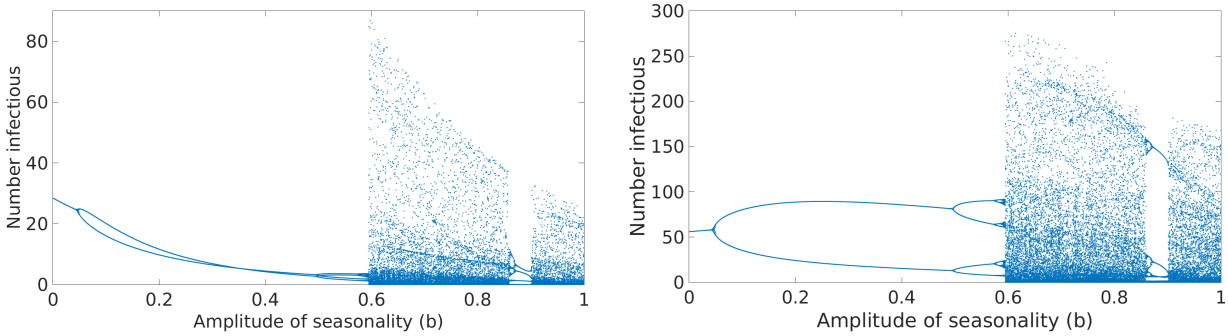

(a) Total number of infectious individuals at the beginning of January against the value of the seasonality amplitude.

(b) Total number of infectious individuals at the beginning of September against the value of the seasonality amplitude.

Figure 1: Bifurcation diagrams for the fractional ageing model in (a) January and (b) early September with sinusoidal seasonal forcing

.

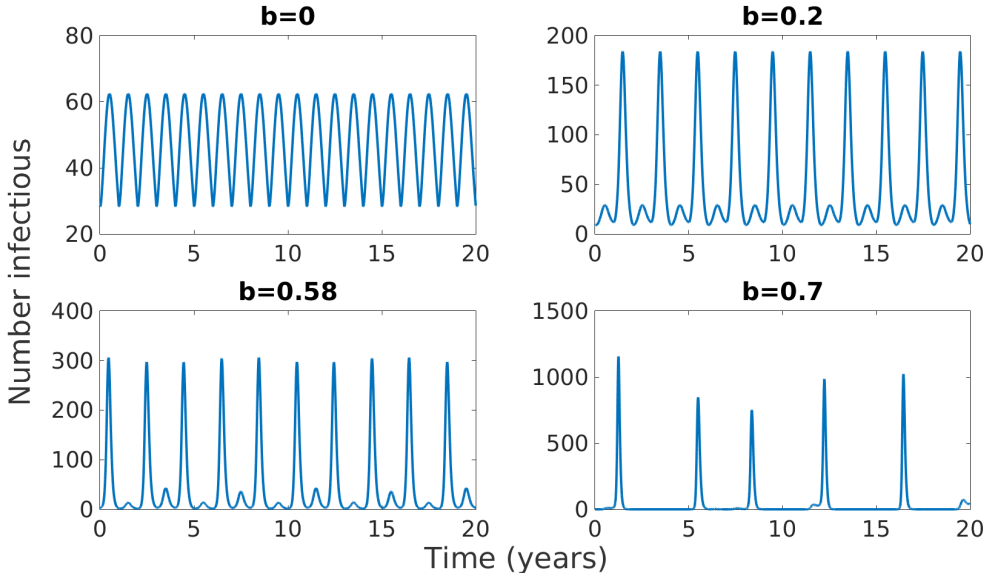

Figure 2: 20 year samples taken from time series of the fractional ageing model with sinusoidal seasonal forcing for a number of values of the amplitude of seasonality, b, after a 1,000 year burn in.

2.2 Cohort ageing model

We now consider a cohort ageing model [31] with seventy-five age classes. The WAIFW matrix, β, is now a 75×75 matrix composed of blocks of the same values $\beta_1, \beta_2, \beta_3$ and β_4 as in the fractional ageing model to simplify comparison between the models. The annual ageing process now completely empties one age cohort into the next, so that the first class has no individuals but is replenished through the birth of susceptibles, and the final class accumulates all individuals over the age of 75 and is only depleted through deaths. The number of susceptibles updates as:

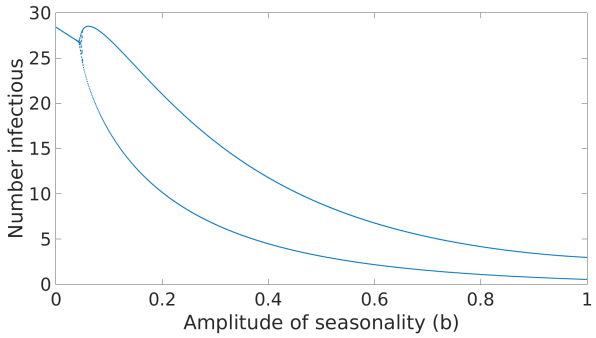

(a) Total number of infectious individuals at the beginning of January against the value of the seasonality amplitude.

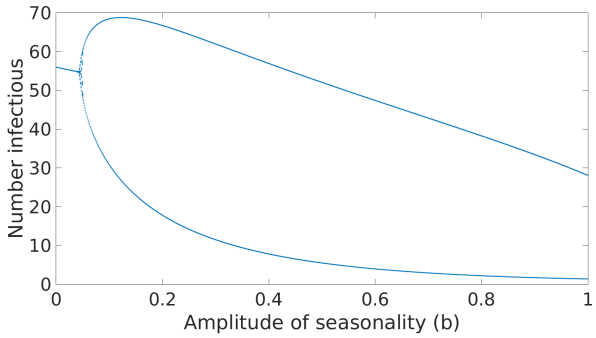

(b) Total number of infectious individuals at the beginning of September against the value of the seasonality amplitude.

Figure 3: Bifurcation diagrams for the fractional ageing model in (a) January and (b) September with term-time seasonal forcing

$$
\begin{aligned}
S_1 &\to 0,\\
S_2 &\to S_1,\\
&\vdots\\
S_{74} &\to S_{73},\\
S_{75} &\to S_{74} + S_{75},
\end{aligned}
$$

and the number of exposed, infectious and recovered individuals update in the same way.

Seasonal forcing can be included in the cohort ageing model by updating the value, β_2, of each entry of the 6×6 block matrix governing interactions between school children in the WAIFW matrix with the time dependent values for sinusoidal (equation 5), and term-time (equation 6) seasonal forcing. Bifurcation diagrams are produced as described in subsection 2.1. The bifurcation diagrams for the cohort ageing model with sinusoidal forcing, shown in figure 4, are significantly different to those for the fractional ageing model in figure 1 – the amplitude of seasonality needs to be much higher to see any variation from the annual dynamics and once the dynamics do change, at an amplitude just below $b = 0.8$, the dynamics become biennial but no further changes in the dynamics are seen as b is varied and in particular, no chaotic dynamics are observed.

Furthermore, the bifurcation diagrams for term-time seasonal forcing of the cohort ageing model, shown in figure 5, appear very different from the fractional ageing model in figure 3. As with the sinusoidal seasonality, the range of amplitudes with annual dynamics is much larger than in the fractional ageing model, and the dynamics become biennial just above $b = 0.4$, multiennial at approximately $b = 0.8$ and then chaotic for larger amplitudes, which contrasts with the fractional ageing model for which chaotic dynamics are not seen. However, for term-time forcing the amplitude does not need to be restricted to $b \in [0, 1]$ so it is possible that the fractional ageing model will display chaotic dynamics for some values $b > 1$, which have not been considered here.

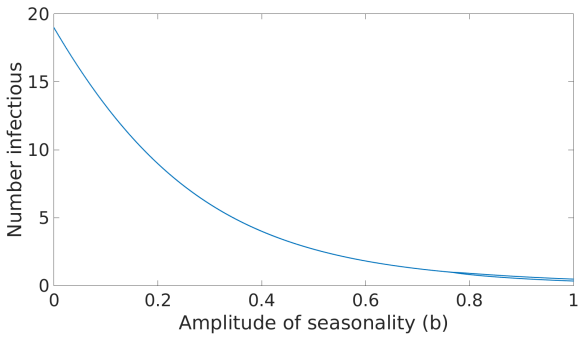

(a) Total number of infectious individuals at the beginning of January against the value of the seasonality amplitude.

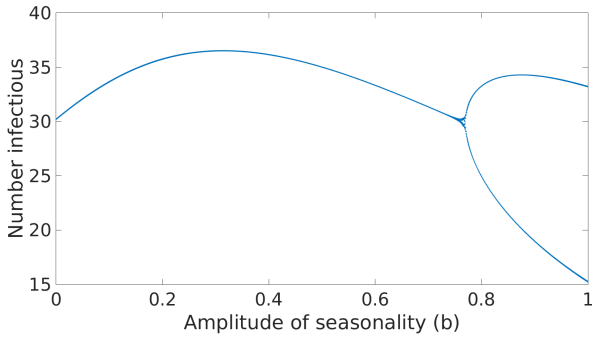

(b) Total number of infectious individuals at the beginning of September against the value of the seasonality amplitude.

Figure 4: Bifurcation diagrams for the cohort ageing model in (a) January and (b) September with sinusoidal seasonal forcing.

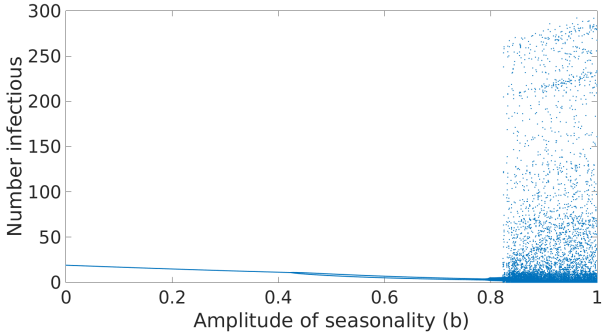

(a) Total number of infectious individuals at the beginning of January against the value of the seasonality amplitude.

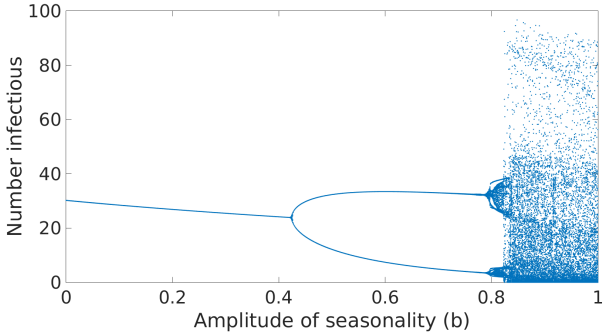

(b) Total number of infectious individuals at the beginning of September against the value of the seasonality amplitude.

Figure 5: Bifurcation diagrams for the cohort ageing model in (a) January and (b) September with term-time seasonal forcing.

3 Data from the 2013 Swansea outbreak

Given a matrix, M, with elements M_{ij} representing the average frequency of contacts an individual of age i has with individuals of age j and a vector of susceptibility $\hat{\beta}$ with the probability of infection by age, the WAIFW matrix is given by

$$\beta = \hat{\beta} M. \tag{8}$$

Therefore, by taking M to be a synthetically produced contact matrix for the UK [13] and calculating the susceptibility vector using vaccination and notification time data from the Swansea outbreak [33] the age structured, seasonally forced model can be fitted to the Swansea outbreak.

The number of notifications of infected individuals against the time since the beginning of the outbreak is approximately exponential, $I(t) \sim \exp(rt)$. Fitting this exponential curve to the data, as shown in figure 6 gives an early growth rate of $r = 0.02265$, which is equivalent to the domi-

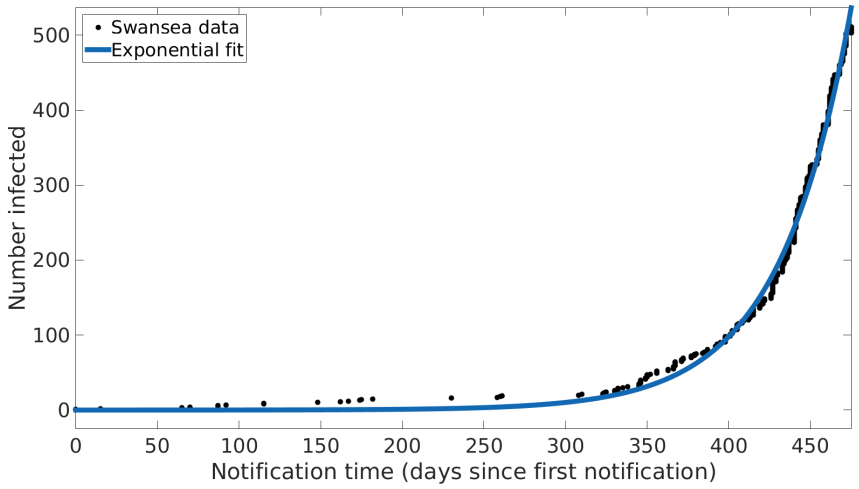

Figure 6: Data on the number of infected individuals against the notification time since the beginning of the outbreak from the 2013 Swansea outbreak of Measles.

nant positive eigenvalue of the disease-free equilibrium [35]. If e_a is the total number of infected individuals in age class a, N_a is the total number of individuals in age class a, υ_a is the percentage of the population of age a who are unvaccinated and $S_a(0) = N_a\upsilon_a/100$ is the initial number of susceptible individuals of age a, then

$$\begin{aligned} re_a &= \sum_b \beta_{ab}\frac{e_b}{N_b}S_a(0) - \gamma e_a \\ &= \sum_b \hat{\beta}_a M_{ab}\frac{e_b}{N_b}S_a(0) - \gamma e_a \end{aligned}$$

$$\Rightarrow \hat{\beta}_a = \frac{(\gamma + r)e_a}{\left(\sum_b M_{ab}\frac{e_b}{N_b}\right)S_a(0)}, \tag{9}$$

where $\hat{\beta}_a$ is the susceptibility to infection of an individual of age a. The overall scaling of the matrix $\beta = \hat{\beta}M$ was then fit to the data in figure 6 and used to once again create bifurcation diagrams, as described in subsection 2.1, but using a cohort ageing model with 90 age classes to fit in with the contact matrix.

The bifurcation diagrams for the data-fitted cohort ageing model with sinusoidal forcing in figure 7 annual dynamics of the same level of infectiousness for all amplitudes of seasonality. The term-time forcing function gave very similar results, with annual dynamics at the same level of infectiousness for all amplitudes, so they have not been included here.

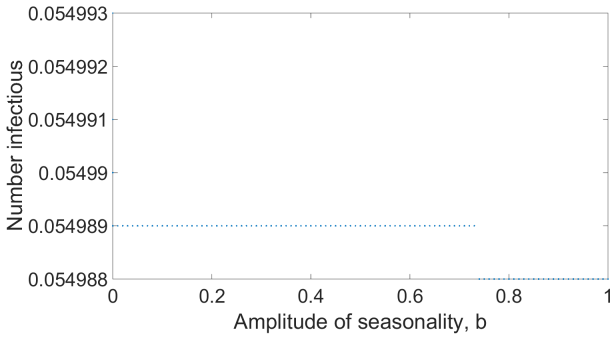

(a) Total number of infectious individuals at the beginning of January against the value of the seasonality amplitude.

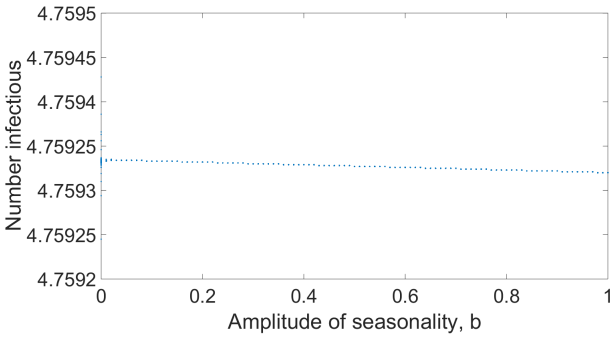

(b) Total number of infectious individuals at the beginning of September against the value of the seasonality amplitude.

Figure 7: Bifurcation diagrams for the cohort ageing model fitted to data from the Swansea 2013 Measles outbreak in (a) January and (b) September with sinusoidal seasonal forcing.

4 Conclusions and further work

Bifurcation diagrams have been used as a tool to compare age structured models with seasonal forcing. When a sinusoidal seasonal forcing term is used, the bifurcation diagrams show a marked difference between the fractional ageing model, which exhibits chaotic dynamics when the amplitude of seasonality is high enough, and the cohort ageing model which does not display chaotic dynamics for any values of the amplitude of seasonality. When the term-time seasonal forcing term is used, the dynamics appear to differ between the two models again. However, the amplitude can take values outside those used here with this form of seasonal forcing, and so the dynamics may be more similar if a larger section of the parameter space for the amplitude is considered. The bifurcation diagrams from the cohort ageing model when fitted to the Swansea data are very different from those produced using the parameters from historical data throughout the rest of the paper, possibly due to fitting a lower value of R_0 to the historical data, and thereby significantly changing the observed dynamics.

Further work could include modifying the age-dependent death rate, D_a, to match mortality data instead of assuming deaths only occur from the final age class, including maternal immunity – where children are not in born into the susceptible class, but with an immunity which is passed on from the mother and lasts approximately six months before reverting to the susceptible class, incorporating spatial heterogeneities and including partial vaccination levels. In addition to this, only one attractor has been considered when comparing bifurcation diagrams here, further work could investigate the existence of other attractors.

References

[1] Anderson, R. M., and May, R. M. Directly transmitted infectious diseases: control by vaccination. *Science 215*, 4536 (1982), 1053–1060.

[2] Anderson, R. M., and May, R. M. Age-related changes in the rate of disease transmission: implications for the design of vaccination programmes. *Journal of Hygiene 94*, 3 (1985), 365–436.

[3] Anderson, R. M., May, R. M., Joysey, K., Mollison, D., Conway, G. R., Cartwell, R., Thompson, H. V., and Dixon, B. The invasion, persistence and spread of infectious diseases within ani-

mal and plant communities [and discussion]. *Philosophical Transactions of the Royal Society of London B: Biological Sciences 314*, 1167 (1986), 533–570.

[4] Aron, J. L., and Schwartz, I. B. Seasonality and period-doubling bifurcations in an epidemic model. *Journal of Theoretical Biology 110*, 4 (1984), 665–679.

[5] Begg, N., Ramsay, M., White, J., and Bozoky, Z. Media dents confidence in MMR vaccine. *BMJ 316*, 7130 (1998), 561.

[6] Bloch, A. B., Orenstein, W. A., Stetler, H. C., Wassilak, S. G., Amler, R. W., Bart, K. J., Kirby, C. D., and Hinman, A. R. Health impact of measles vaccination in the United States. *Pediatrics 76*, 4 (1985), 524–532.

[7] Bolker, B. Chaos and complexity in measles models: a comparative numerical study. *Mathematical Medicine and Biology 10*, 2 (1993), 83–95.

[8] Davidkin, I., and Valle, M. Vaccine-induced measles virus antibodies after two doses of combined measles, mumps and rubella vaccine: a 12-year follow-up in two cohorts. *Vaccine 16*, 20 (1998), 2052–2057.

[9] Earn, D. J., Rohani, P., Bolker, B. M., and Grenfell, B. T. A simple model for complex dynamical transitions in epidemics. *Science 287*, 5453 (2000), 667–670.

[10] Fine, P., Eames, K., and Heymann, D. L. "Herd immunity": a rough guide. *Clinical infectious diseases 52*, 7 (2011), 911–916.

[11] FINE, P. E., and CLARKSON, J. A. Measles in England and Wales—I: An analysis of factors underlying seasonal patterns. *International Journal of Epidemiology 11*, 1 (1982), 5–14.

[12] Finkenstädt, B. F., and Grenfell, B. T. Time series modelling of childhood diseases: a dynamical systems approach. *Journal of the Royal Statistical Society: Series C (Applied Statistics) 49*, 2 (2000), 187–205.

[13] Fumanelli, L., Ajelli, M., Manfredi, P., Vespignani, A., and Merler, S. Inferring the structure of social contacts from demographic data in the analysis of infectious diseases spread. *PLoS Comput Biol 8*, 9 (2012), e1002673.

[14] Gastañaduy, P. A., Redd, S. B., Fiebelkorn, A. P., Rota, J. S., Rota, P. A., Bellini, W. J., Seward, J. F., and Wallace, G. S. Measles — United States, January 1– May 23, 2014. *MMWR Morb Mortal Wkly Rep 63*, 22 (2014), 496–499.

[15] Iacobucci, G. Wales sets up drop-in vaccination clinics to tackle measles outbreak. *BMJ 346* (2013).

[16] Jakab, Z., and Salisbury, D. M. Back to basics: the miracle and tragedy of measles vaccine. *The Lancet 381*, 9876 (2013), 1433–1434.

[17] Keeling, M. J. Modelling the persistence of measles. *Trends in microbiology 5*, 12 (1997), 513–518.

[18] Keeling, M. J., and Grenfell, B. Disease extinction and community size: modeling the persistence of measles. *Science 275*, 5296 (1997), 65–67.

[19] Keeling, M. J., Rohani, P., and Grenfell, B. T. Seasonally forced disease dynamics explored as switching between attractors. *Physica D: Nonlinear Phenomena 148*, 3 (2001), 317–335.

[20] Kermack, W. O., and McKendrick, A. G. A contribution to the mathematical theory of epidemics. *Proceedings of the Royal Society of London A: Mathematical, Physical and Engineering Sciences 115*, 772 (1927), 700–721.

[21] London, W. P., and Yorke, J. A. Recurrent outbreaks of measles, chickenpox and mumps I. Seasonal variation in contact rates. *American journal of epidemiology 98*, 6 (1973), 453–468.

[22] Majumder, M. S., Cohn, E. L., Mekaru, S. R., Huston, J. E., and Brownstein, J. S. Substandard vaccination compliance and the 2015 measles outbreak. *JAMA Pediatrics 169*, 5 (2015), 494–495.

[23] Mason, B., and Donnelly, P. Impact of a local newspaper campaign on the uptake of the measles mumps and rubella vaccine. *Journal of epidemiology and community health 54*, 6 (2000), 473–474.

[24] May, R. M., and Anderson, R. M. Spatial heterogeneity and the design of immunization programs. *Mathematical Biosciences 72*, 1 (1984), 83–111.

[25] McLean, A., and Anderson, R. Measles in developing countries Part I. Epidemiological parameters and patterns. *Epidemiology and Infection 100*, 1 (1988), 111–133.

[26] Papania, M. J., Wallace, G. S., Rota, P. A., Icenogle, J. P., Fiebelkorn, A. P., Armstrong, G. L., Reef, S. E., Redd, S. B., Abernathy, E. S., Barskey, A. E., et al. Elimination of endemic measles, rubella, and congenital rubella syndrome from the Western hemisphere: the US experience. *JAMA pediatrics 168*, 2 (2014), 148–155.

[27] Public Health England. Evaluation of vaccine uptake during the 2013 MMR catch-up campaign in england. `https://www.gov.uk/government/uploads/system/uploads/attachment_data/file/285890/Evaluation_of_the_2013_MMR_catch-up_campaign_in_England.pdf`, 2014. [Online; accessed 14-September-2015].

[28] Ramsay, M., Brugha, R., and Brown, D. Surveillance of measles in England and Wales: implications of a national saliva testing programme. *Bulletin of the World Health Organization 75*, 6 (1997), 515–521.

[29] Ramsay, M. E. Measles: the legacy of low vaccine coverage. *Archives of disease in childhood 98*, 10 (2013), 752–754.

[30] Sabella, C. Measles: not just a childhood rash. *Cleveland Clinic journal of medicine 77*, 3 (2010), 207–213.

[31] Schenzle, D. An age-structured model of pre- and post-vaccination measles transmission. *Math Med Biol 1*, 2 (1984), 169–191.

[32] Soper, H. E. The interpretation of periodicity in disease prevalence. *Journal of the Royal Statistical Society 92*, 1 (1929), 34–73.

[33] Temple, M. Personal correspondence (August 2015).

[34] Watson, J. C., Hadler, S. C., Dykewicz, C. A., Reef, S., and Phillips, L. Measles, mumps, and rubella – vaccine use and strategies for elimination of measles, rubella, and congenital rubella syndrome and control of mumps: Recommendations of the Advisory Committee on Immunization Practices (ACIP). *MMWR Recommendations and Reports 47*, RR-8 (1998), 1–57.

[35] Wearing, H. J., Rohani, P., and Keeling, M. J. Appropriate models for the management of infectious diseases. *PLoS medicine 2*, 7 (2005), 621.

[36] Wise, J. Largest group of children affected by measles outbreak in Wales is 10–18 year olds. *BMJ 346* (2013).

[37] World Health Organisation. Measles (MCV) data by country. `http://apps.who.int/gho/data/node.main.A826`, 2015. [Online; accessed 14-September-2015].

[38] World Health Organization. WHO position on measles vaccines. *Vaccine 27*, 52 (2009), 7219–7221.

[39] YORKE, J. A., and LONDON, W. P. Recurrent outbreaks of measles, chickenpox and mumps II. Systematic differences in contact rates and stochastic effects. *American Journal of Epidemiology 98*, 6 (1973), 469–482.